Asian Journal of Chemistry; Vol. 25, No. 10 (2013), 5811-5815

ASIAN JOURNAL OF CHEMISTRY

http://dx.doi.org/10.14233/ajchem.2013.OH98

Surface Characteristics and Photocatalytic Gas Degradation of Nonmetal Element-Doped Titania†

WAN-KUEN JO

Department of Environmental Engineering, Kyungpook National University, 80 University Road, Bukgu, Daegu 702-701, Republic of Korea

Corresponding author: Fax: +82 53 9506579; Tel: +82 53 9506584; E-mail: wkjo@knu.ac.kr

AJC-13341

The present study explored the characteristics and the photocatalytic activities of S-doped TiO_2 (S-TiO_2) and N-doped TiO_2 (N-TiO_2) for the decomposition of gas-phase isopropyl alcohol, according to calcination temperatures. The characteristics of the prepared photocatalysts were determined using an X-ray diffractometer, a scanning electron microscope, a diffuse reflectance ultraviolet-visible-near infrared spectrophotometer, and a Fourier-transform infrared spectrometer. The average degradation efficiency of isopropyl alcohol by the S-TiO_2 calcined at 350 ºC was 40 %, whereas it was 98 % for the S-TiO_2 calcined at 550 ºC. However, the average degradation efficiency of isopropyl alcohol decreased to 92 % when the calcination temperature was further increased from 550 to 650 ºC. The average degradation efficiency of isopropyl alcohol by the N-TiO_2 calcined at 350 ºC was 93 %, whereas it was close to 100 % for the N-TiO_2 calcined at 550 and 650 ºC. Moreover, the acetone generation yields as determined using the S- and N-TiO_2 were 86 and 58 %, respectively, for the calcination temperature of 350 ºC, whereas they were 78 and 69 %, respectively, for the calcination temperature of 650 ºC. Consequently, as-prepared S-TiO_2 and N-TiO_2 photocatalysts could be applied to purification of airborne isopropyl alcohol under visible-light irradiation, but the formation of acetone should be considered for their applications.

Key Words: Isopropyl alcohol, Calcination temperature, N-doped, S-doped, Acetone generation.

INTRODUCTION

Among several semiconductors, titanium dioxide (TiO_2) is the most commonly employed photocatalyst due to inexpensive cost, readily availability, and chemical stability[1,2]. However, TiO_2 exhibits a relatively high activity only under UV light, which exceeds the band-gap energy of 3.0 or 3.2 eV in the rutile or anatase crystalline phase, respectively, limiting its practical applications[3]. Modification of photocatalysts for the enhancement of light absorption and photocatalytic activity under visible light irradiation has been the focus of recent studies. Several methods, such as dye sensitization[4,5], transition metals doping[6,7] and non-metal doping[8-11] have been proposed to modify the electronic properties of bulk TiO_2. In particular, TiO_2 photocatalysts impregnated with non-metal elements, such as sulfur (S) and nitrogen (N), have received more recent attention as one of the most attractive photocatalyst groups that exhibit relatively high activities under visible light[8-11].

It is noteworthy that calcination temperature of a photocatalyst for a preparation process can be an important factor, which influences its surface characteristics and thus, its photocatalytic activities[12,13]. As compared with unmodified TiO_2, this kind of study was much less reported for nonmetal element-doped photocatalysts in literature. This assertion has led the present study to investigate the effects of calcinations temperatures of the element-doped photocatalysts on surface characteristics and photocatalytic activities for environmental applications. Accordingly, the current study utilized two different types of photocatalysts, S element-doped TiO_2 (S-TiO_2) and N element-doped TiO_2 (N-TiO_2), for the decomposition of gas-phase isopropyl alcohol also called 2-propanol, according to calcination temperatures. The target compounds, isopropyl alcohol is generally detected at higher concentration levels in indoor than outdoor environments[14]. In addition, this compound is a prototype VOC for photocatalytic studies because the initial reaction pathway involves almost exclusively the partial oxidation to acetone[15].

EXPERIMENTAL

S-doped and N-doped photocatalysts: S-TiO_2 powders were prepared by mixing titanium isopropoxide (100 g) with thiourea (107.2 g) at a molar ratio of 1:4 in ethanol (1,000 mL). The solution was stirred at room temperature for 1 h, and after the evaporation of ethanol, a white slurry was obtained. After leaving the slurry for 3 days at room temperature (between 18 and 23 ºC), a white powder was obtained. This

†Presented to the 6th China-Korea International Conference on Multi-functional Materials and Application, 22-24 November 2012, Daejeon, Korea

powder was calcined at 350, 450, 550 or 650 ºC for 1 h under aerated conditions to obtain a yellow powder.

N-TiO_2 photocatalysts were prepared utilizing urea as an N source for mechanical N-doping. Eight gram of commercially available TiO_2 powder (Degussa P-25) was added to 20 mL of aqueous solution of the organic nitrogen compound (urea) and stirred at room temperature for 1 h. The mixture was kept in the dark for 1 day and then dried under reduced pressure. N-doped TiO_2 powder was calcined at 350, 450, 550, or 650 ºC for 1 h under aerated conditions to obtain yellow powder. The calcined powder was washed with diluted sulfuric acid and then with pure water, and vacuum-dried. The pH of the final solution was 7.

The prepared S-TiO_2 and N-TiO_2 powders were characterized using an X-ray diffractometer, a scanning electron microscope, a diffuse reflectance ultraviolet-visible-near infrared (UV-VIS-NIR) spectrophotometer, a Fourier-transform infrared spectrometer. XRD patterns were determined on a Rigaku D/max-2500 diffractometer with CuK_α radiation operated at 40 kV and 100 mA. The particle morphology was observed using a Hitachi S-4300 & EDX-350 FE-SEM at an acceleration voltage of 15 kV. Visible absorption spectra were obtained for the dry pressed disk samples using a Varian CARY 5G spectrophotometer equipped with an integrating sphere. Polytetrafluoroethylene was used as a reference. FTIR analysis was performed on a PerkinElmer Spectrum GX spectrophotometer at a resolution of 4 cm^{-1} in the spectral range of 4000-400 cm^{-1}, using a KBr pellet for sample preparation.

The photocatalytic reactor was constructed using two Pyrex tubes with different diameters but with a same length (26.5 cm). A conventional lamp was inserted inside the smaller-diameter Pyrex tube. The inner wall of the outer Pyrex tube was coated with a thin film of the N-TiO_2 or S-TiO_2 photocatalyst. The reactor was designed to direct the flow of incoming air toward the UV light in order to increase the air turbulence inside the reactor, thereby enhancing the distribution of the target compounds onto the photocatalyst surface. The standard gas (0.1 ppm) was prepared by injecting standard isopropyl alcohol into a mixing chamber *via* a syringe pump (Model 210, KdScientific Inc.). The prepared gas was flowed through the annular region between the two Pyrex tubes. Its humidity level was adjusted by passing zero-grade air through a charcoal filter, followed by a humidification device in a water bath. The flow rate was controlled using rotameters calibrated against a dry test meter.

The photocatalytic activities of N-TiO_2 and S-TiO_2 powders prepared at different calcinations temperature were evaluated at specified operational conditions. Four different calcinations temperatures tested were 350, 450, 550 and 650 ºC. Other parameters were fixed to their representative values: calcinations temperature, 350 ºC; IC, 0.1 ppm; RH, 50-55 %; and flow rate, 0.5 L min^{-1}. In addition, the generation yields of a major byproduct (acetone) that could be formed during the photocatalytic processes were determined.

For the evaluation of the photocatalytic activities and acetone generation, a time series of gaseous measurements were collected at the inlet and outlet of the photocatalytic system prior to and after turning on the lamp. Prior to turning on the lamp, six 10-min samples were collected at 1 h interval for 3 h. After 3 h, the introduction of the target compounds (after adsorption equilibrium), the lamp was turned on and another series of six 10-min samples were collected at 1 h interval for 3 h. The catalyst was pretreated for several hours by making zero-grade air flow through the illuminated reactor. The catalyst pretreatment was performed after the humidity level at the reactor outlet reached equilibrium. When no contamination with the target compounds was measured in the reactor, the target compounds were introduced.

Gas samples were collected by filling an evacuated 5-L Tedlar bag at a constant flow rate. Air from this bag was then drawn through a sorbent trap containing 0.3 gof Tenax TA using a constant flow-sampling pump (A.P. Buck Inc. Model I.H). All samples were taken at ambient room temperature (19-25 ºC). The target compounds collected on the sorbent trap were analyzed by coupling a thermal desorption system (SPIS TD, Donam Inc.) to a gas chromatograph (Agilent 7890A) with a flame ionization detector using a 0.32-mm-i.d. by 60-m-length fused silica column (SPB-5, Supelco Co.). The quality assurance/quality control program for the measu-rement of target compounds included laboratory blank traps and spiked samples.

RESULTS AND DISCUSSION

Characteristics of S-TiO_2 and N-TiO_2: The particle morpho-logies of S-TiO_2 and N-TiO_2 were observed utilizing XRD patterns, SEM images, UV-visible spectroscopy, and FTIR patterns. Fig. 1 illustrates the XRD patterns of both S-TiO_2 and N-TiO_2 photocatalysts calcined at four different temperatures (350, 450, 550 and 650 ºC), which were represented as S-350 and N-350, S-450 and N-450, S-550 and N-550, and S-650 and N-650, respectively. The photocatalysts prepared at different calcination temperatures revealed different XRD patterns. For both types of S-TiO_2 and N-TiO_2 photocatalysts, the peak intensity of anatase ($2\theta = 25.2°$) decreased and the width plane became narrow, as the calcination temperature increased from 350 to 650 ºC. On the other hand the peak intensity of rutile ($2\theta = 27.4°$) increased with increasing calcination temperature. Therefore, the phase transformation from anatase to rutile would increase as calcination temperature was increased[16,17]. The increasing trend in rutile contents with increased calcination temperature was consistent with that of S-TiO_2 prepared using a hydrolysis method by other researchers[17]. It is notable that the locations for major XRD peaks were nearly same for the two types of photocatalysts, although their intensities were not. These findings are likely due to the low amounts of sulfur and nitrogen in the S-TiO_2 and N-TiO_2 photocatalysts, respectively.

Fig. 2 presents the SEM images of S-TiO_2 and N-TiO_2 photocatalysts calcined at different temperatures. These images show a clear difference in microstructures of photocatalysts prepared at different calcination temperatures. For both S-TiO_2 and N-TiO_2, the particle size increased apparently as calcination temperature was increased. This is attributed to the phase transformation from anatase to larger particle size of rutile with increasing calcination temperature as proved previously in the XRD patterns. Han *et al.*[1] also reported a similar size dependence on calcination temperature of their S-TiO_2 powders.

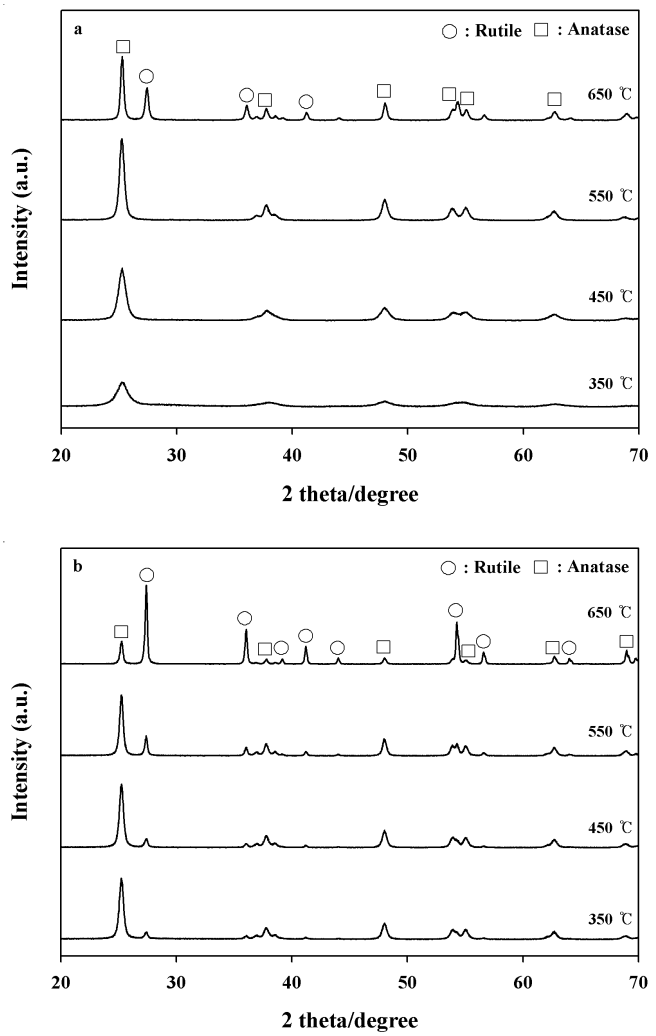

Fig. 1. XRD pattern of photocatalysts at calcinations temperature of 350, 450, 550 and 650 ºC: a, S-TiO_2; and b, N-TiO_2

Higher agglomeration was observed for N-TiO_2 as compared to the S-TiO_2 sample. These findings are supported by a hypothetical theory that sulfur species in S-doped TiO_2 could improve dispersion, thereby lowering agglomerate size[18].

Fig. 3 exhibits the UV-visible absorbance spectra of both S-TiO_2 and N-TiO_2 prepared at different calcination temperatures. Several studies[19-21] have reported that unmodified TiO_2 photocatalysts exhibited the absorption edge at $\lambda \approx 430$ nm.

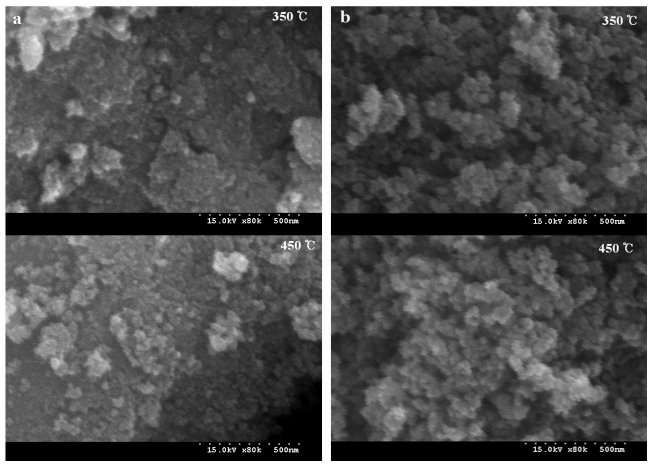

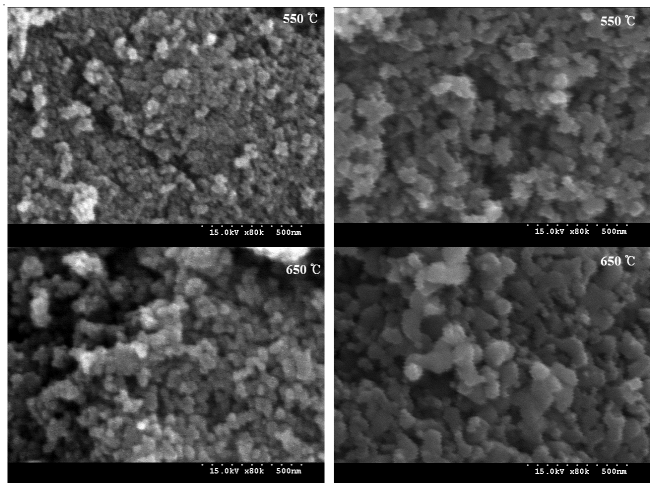

Fig. 2. SEM image photocatalysts at calcination temperature of 350, 450, 550 and 650 ºC: a, S-TiO_2; and b, N-TiO_2

However, for all the prepared S-TiO_2 photocatalysts, the light absorption region was extended to the visible-light range. In particular, S-350 showed the highest light absorption in the visible region (500-800 nm). This light absorption shift for S-TiO_2 was also reported by other studies[9,22,23]. The absorption edge for the S-TiO_2 photocatalysts shifted to $\lambda = 800$ nm was attributed to S element doped into TiO_2 particles[22,23]. Similar to S-TiO_2 photocatalysts, all the N-TiO_2 photocatalysts prepared at four different calcination temperatures also exhibited the shift of the light absorption edge to the visible range, which was consistent with that of other studies[8,19]. For this case, the N-350 revealed the highest light absorption in the visible region (400-800 nm). The shift in the absorption edge for the N-TiO_2 photocatalysts was also ascribed to N element incorporated into the bulk phase of TiO_2[19]. Consequently, it was identified that S or N atoms could be incorporated into two different sites of the bulk phase of TiO_2, regardless of calcination temperatures. These findings further suggested that the prepared S-TiO_2 and N-TiO_2 photocatalysts could be activated effectively by visible-light irradiation. Meanwhile, a higher N-TiO_2 absorbance level was obtained in all visible regions, in comparison to the S-TiO_2 result. However, it is noteworthy that this pattern may be reversed, depending on the synthesis routes of the two types of photocatalysts.

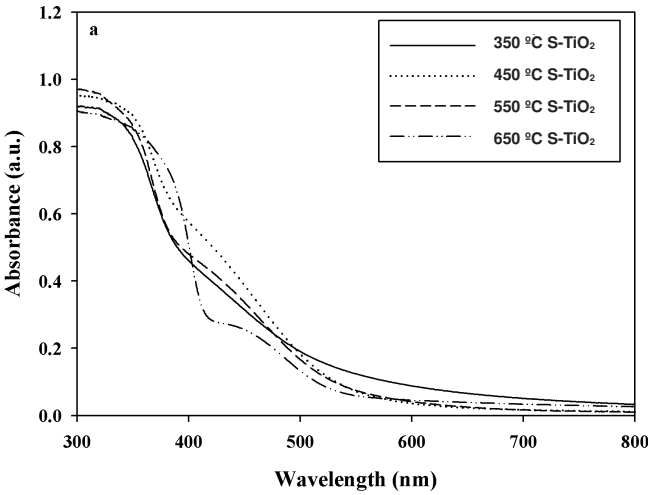

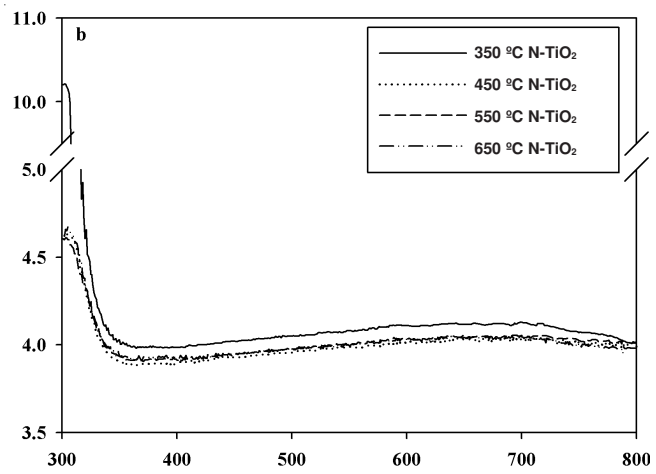

Fig. 3. UV-visible spectra of photocatalysts at calcination temperature of 350, 450, 550 and 650 ºC: a, S-TiO_2 and b, N-TiO_2

Photocatalytic activities of S-TiO_2 and N-TiO_2: Figs. 4a and 5a present the photocatalytic degradation efficiencies for isopropyl alcohol obtained from the photocatalytic units with S-TiO_2 and N-TiO_2 photocatalysts, respectively, according to calcination temperature. Regarding both types of photocatalysts, the degradation efficiency of isopropyl alcohol increased as the calcination temperature increased from 350 to 550 ºC. The average degradation efficiency of isopropyl alcohol by the S-350 was 40 %, whereas it was 98 % for the S-550. However, the average degradation efficiency of isopropyl alcohol decreased to 92 % when the calcination temperature was further increased from 550 to 650 ºC. The average degradation efficiency of isopropyl alcohol by the N-350 was 93 %, whereas it was close to 100 % for both the N-550 and N-650. These findings are ascribed to the combined effects of the ratios of anatase to rutile phase and surface areas of the photocatalysts, which were prepared at different calcination temperatures, on photocatalytic degradation efficiency of isopropyl alcohol. The ratios of anatase to rutile phase would decrease as calcination temperature increased, since, as shown in the XRD results, more phase transformation from anatase to rutile were occurred when calcination temperature was incresed. These anatase to rutile ratios are closely associated with the recombination of electron-hole recombination, which influence the degradation efficiency of photocatalysts[16,17]. Moreover, as presented in the SEM images, the particle size of S-TiO_2 and N-TiO_2 increased as calcination temperature increased, which would also influence photocatalytic degradation efficiencies of isopropyl alcohol.

Figs. 4b and 5b shows the yields of acetone, which was generated during the photocatalytic processes of isopropyl alcohol, obtained from the photocatalytic units with S-TiO_2 and N-TiO_2 photocatalysts, respectively. The acetone yields were estimated by comparing the concentration of acetone generated during the photocatalytic processes of isopropyl alcohol and the concentration of isopropyl alcohol converted. Unlike the degradation efficiencies of isopropyl alcohol, the acetone generation yields determined *via* the S-TiO_2 slightly decreased as the calcination temperature increased, while those of N-TiO_2 exhibited a slight increasing trend. The acetone generation yields as determined using the S-TiO_2 and N-TiO_2 were 86 and 58 %, respectively, for the calcination temperature of 350 ºC, whereas they were 78 and 69 %, respectively, for the calcination temperature of 650 ºC. Consistently, previous studies[15,24] have reported the formation of acetone as the principal byproduct during the photocatalytic oxidation of isopropyl alcohol under specified conditions. The acetone molecules are formed from photocatalytic dehydrogenation of hydrogen bonded isopropyl alcohol molecules, whereas chemisorbed 2-propoxy species could be preferentially oxidized directly to CO_2[24].

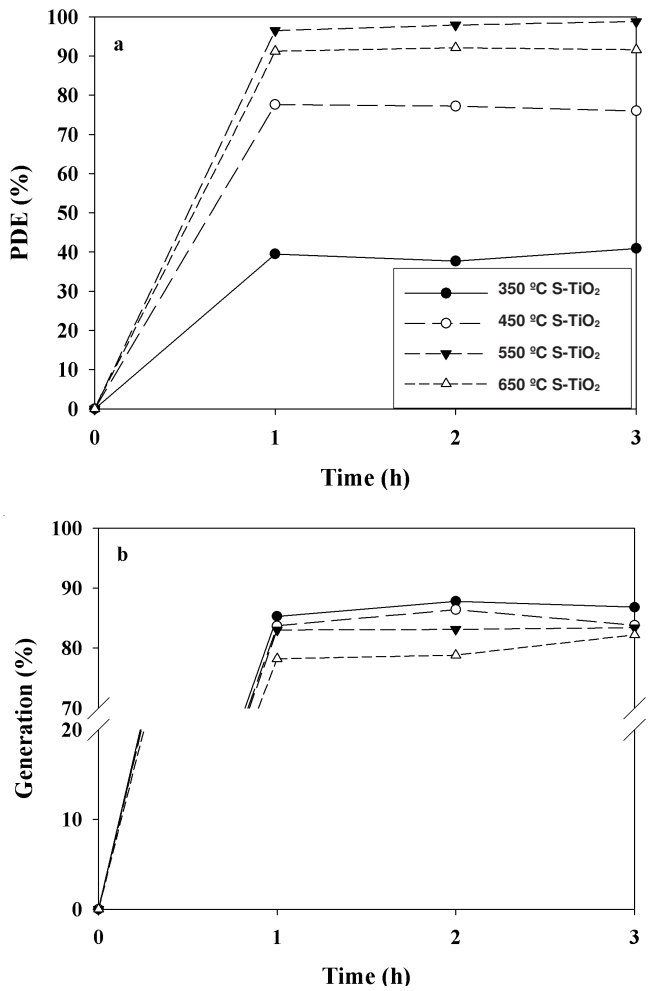

Fig. 4. Photocatalytic decomposition efficiency (PDE) of isopropyl alcohol (a) and generation yields of acetone (b) as determined *via* a photocatalytic system with S-TiO_2, according to calcination temperature

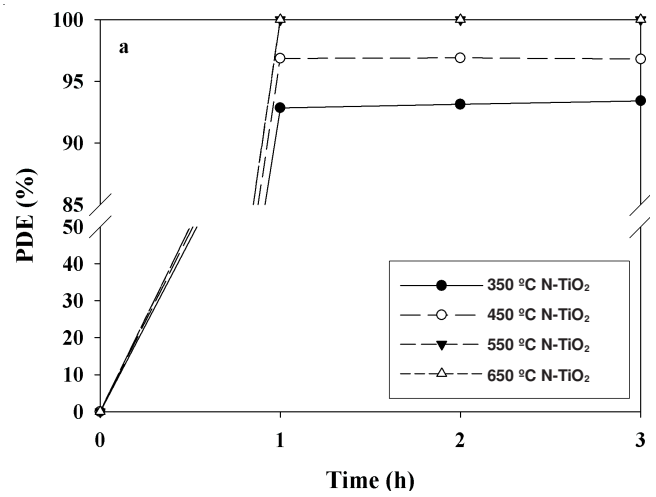

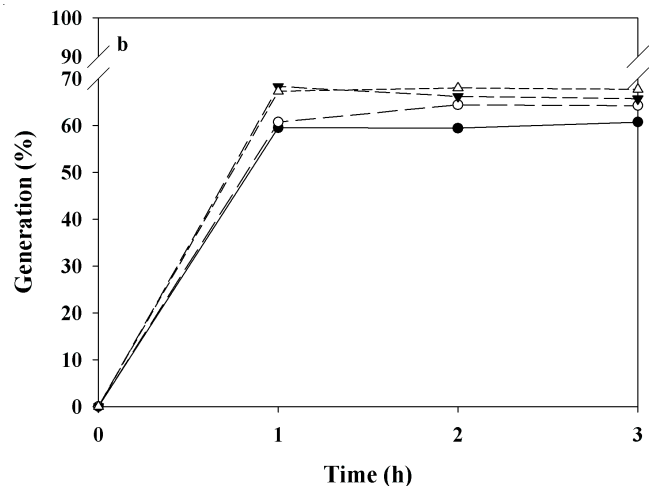

Fig. 5. Photocatalytic decomposition efficiency (PDE) of isopropyl alcohol (a) and generation yields of acetone (b) as determined *via* a photocatalytic system with N-TiO_2, according to calcination temperature

Fig. 6 shows the comparison of S-TiO_2 and N-TiO_2 photocatalysts for their isopropyl alcohol photocatalytic degradation. Under visible-light irradiation, the degradation efficiency of isopropyl alcohol was much higher for the N-TiO_2 than for the S-TiO_2. The degradation efficiency for the N-TiO_2 was between 93 %, while that for the S-TiO_2 was between 40 %. Furthermore, the degradation efficiency by the N-doped TiO_2 was well above 90 % for all the photocatalysts calcined between 350 and 650 ºC. Nevertheless, it is noteworthy that the results of comparison between the two types of element-doped photocatalysts (S-TiO_2 and N-TiO_2) for degradation efficiencies of isopropyl alcohol may not be applicable to different experimental conditions, because degradation efficiencies of isopropyl alcohol depend on the preparation conditions of these photocatalysts, including the amounts of elements and synthesis routes.

Conclusion

This study examined the characteristics and the photocatalytic activities of S-TiO_2 and N-TiO_2 for the decomposition of gas-phase isopropyl alcohol. The surface characteristics of both photocatalysts showed a calcination temperature dependence. It was notable that the locations for major XRD peaks were nearly same for the two types of photocatalysts, although their intensities were not, which was likely due to the low amounts of sulfur and nitrogen in the S-TiO_2 and N-TiO_2 photocatalysts, respectively. It was also suggested that sulfur species in S-doped TiO_2 could improve dispersion, thereby lowering agglomerate size. The as-prepared photocatalysts exhibited the extension of the light absorption region into the visible range. Regarding both types of photocatalysts, the degradation efficiency of isopropyl alcohol increased as the calcination temperature increased, under visible-light irradiation. The present study further confirmed the formation of acetone as the principal byproduct during the photocatalytic oxidation of isopropyl alcohol. Consequently, as-prepared S-TiO_2 and N-TiO_2 photocatalysts could be applied to purification of airborne isopropyl alcohol under visible-light irradiation, but the formation of acetone should be considered for their applications.

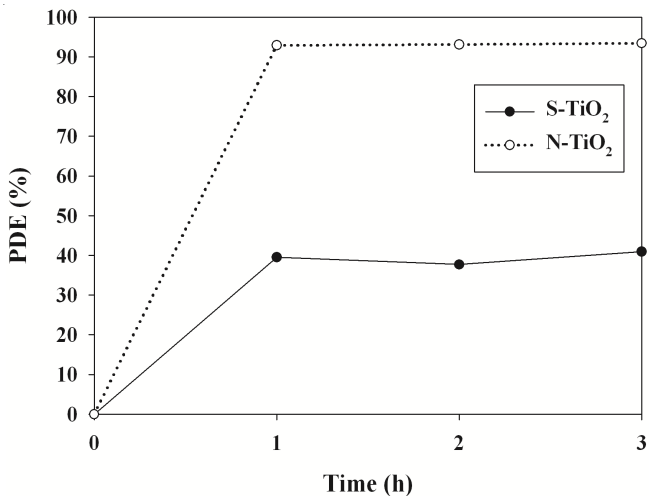

Fig. 6. Comparison of photocatalytic decomposition efficiencies of isopropyl alcohol as determined *via* photocatalytic systems with S-TiO_2 and N-TiO_2, calcined at a temperature of 350 ºC

ACKNOWLEDGEMENTS

This work was supported by the National Research Foundation of Korea (NRF) grant funded by the Korean Government (MEST) (No. 2011-0027916).

REFERENCES

1. C. Han, M. Palaez, V. Likodimos, A.G. Kontos, P. Falaras, K. O'Shea and D.D. Dionysiou, *Appl. Catal. B*, **107**, 77 (2011).
2. Y. Paz, *Appl. Catal. B*, **99**, 448 (2010).
3. D. Chatterjee and S. Dasgupta, *J. Photochem. Photobiol. C*, **6**, 186 (2005).
4. H. Ding, H. Sun and Y. Shan, *J. Photochem. Photobiol.*, **169**, 101 (2005).
5. O. Ozcan, F. Yukruk, E.U. Akkaya and D. Uner, *Appl. Catal. B*, **71**, 291 (2007).
6. H. Chun, T. Yuchao and T. Hongxiao, *Catal. Today*, **90**, 325 (2004).
7. M.A. Rauf, M.A. Meetani and S. Hisaindee, *Desalination*, **276**, 13 (2011).
8. K. Yamada, H. Yamane, S. Matsushima, H. Nakamura, K. Ohira, M. Kouya and K. Kumada, *Thin Solid Films*, **516**, 7482 (2008).
9. M.R. Bayati, A.Z. Moshfegh and F. Golestani-Fard, *Appl. Catal. A*, **89**, 60 (2010).
10. W.K. Jo and C.H. Yang, *Build. Environ.*, **45**, 819 (2010).
11. H. Sun, S. Wang, H.M. Ang, M.O. Tade and Q. Li, *Chem. Eng. J.*, **162**, 437 (2010).
12. N. Mahdjoub, N. Allen, P. Kelly and V. Vishnyakov, *J. Photochem. Photobiol. A*, **211**, 59 (2010).
13. A.M. Luís, M.C. Neves, M.H. Mendonça and O.C. Monteiro, *Mater. Chem. Phys.*, **125**, 20 (2011).
14. C. Jia, S. Batterman and C. Godwin, *Atmos. Environ.*, **42**, 2101 (2008).
15. D. Vildozo, C. Ferronato, M. Sleiman and J.-M. Chovelon, *Appl. Catal. B*, **94**, 303 (2010).
16. N. Venkatachalam, M. Palanichamy and V. Murugesan, *Mater. Chem. Phys.*, **104**, 454 (2007).
17. H. Znad and Y. Kawase, *J. Mol. Catal. A*, **314**, 55 (2009).
18. S. Liu and X. Chen, *J. Hazard. Mater.*, **152**, 48 (2008).
19. T. Horikawa, M. Katoh and T. Tomida, *Micropor. Mesopor. Mater.*, **110**, 397 (2008).
20. W.K. Jo and J.T. Kim, *J. Hazard. Mater.*, **164**, 360 (2009).
21. X. Qin, L. Jing, G. Tian, Y. Qu and Y. Feng, *J. Hazard. Mater.*, **172**, 1168 (2009).
22. T. Ohno, M. Akiyoshi, T. Umebayashi, K. Asai, T. Mitsui and M. Matsumura, *Appl. Catal. A*, **265**, 115 (2004).
23. S.H. Nam, T.K. Kim and J.H. Boo, *Catal. Today*, **185**, 259 (2012).
24. M.D. Hernández-Alonso, I. Tejedor-Tejedor, J.M. Coronado, M.A. Anderson and J. Soria, *Catal. Today*, **143**, 364 (2009).